INSTITUTE OF PHYSICS PUBLISHING JOURNAL OF PHYSICS D: APPLIED PHYSICS

J. Phys. D: Appl. Phys. **38** (2005) 2215–2226 doi:10.1088/0022-3727/38/13/021

Charge–voltage relationship of the first impulse corona in long airgaps

P Ortéga[1], F Heilbronner[2], F Rühling[2], R Díaz[3] and M Rodière[1]

[1] Laboratoire Terre-Océan, University of French Polynesia, BP 6570, 98702 Faaa, French Polynesia
[2] Institute of High Voltage Engineering and Electric Power Transmission, Technical University of Munich, D-80290 München, Germany
[3] High Voltage Laboratory, Institute of Electrical Engineering, National University of Tucuman, 4000 SM Tucuman, Argentina

E-mail: ortega@upf.pf, falk.ruehling@tum.de and rdiaz@herrera.unt.edu.ar

Received 20 December 2004, in final form 1 April 2005
Published 17 June 2005
Online at stacks.iop.org/JPhysD/38/2215

Abstract
This paper investigates the relationship between the charge Q_i of the first impulse corona and the associated inception voltage U_i for a 1 m point–plane airgap submitted to impulse voltages. Experimental studies under both polarities are reported; the Q_i–U_i characteristics obtained allow empirical quadratic relationships between these two quantities to be derived. A physical interpretation is proposed by considering the established characteristics of the first impulse corona. The Gauss and Ampère–Maxwell laws can be applied and the quadratic Q_i–U_i relationship is justified by the present model.

List of symbols

A	constant used in the charge density expression ($C\,m^{-2}$)
a	constant in equation (21)
au	arbitrary unit
b	constant in space charge density
B	magnetic field
C	closed curve used for the Ampère–Maxwell law integration
c	constant in space charge density
D	gap length
dc	direct current
E	total electric field
E_g	axial geometric field
E_{gL}	axial geometric field at $r = L$
E_{gs}	guiding field ahead of the streamer system
$E_{i,o}$	minimum field on surface electrode for corona inception
E_s	mean electric field along the streamers[4]
h	absolute humidity ($g\,m^{-3}$)
HV	high voltage
I	current signal recorded during the first corona development
I_{peak}	maximum of I
I_{PM}	current trace of photomultiplier
k	coefficient used in the first charge voltage relationship[4]
k'	coefficient used in the second charge voltage relationship[4]
L	distance from O to the extremity of the streamer, approximate streamer length
N	number of streamers
O	centre of the tip curvature; centre of the spherical coordinates.
Q_c	actual charge deposited by the first corona in the airgap
Q_e	charge induced by the first corona at the HV electrode
Q_i	apparent charge measured during the first corona development
PM	photomultiplier
R	tip radius of the HV electrode
R'	radius of the inner surface considered for the Gauss law integration
r	first spherical coordinate
S_i	inner surface used for the Gauss law integration
S_e	external surface used for the Gauss law integration
S_ℓ	lateral surface used for the Gauss law integration

[4] These can be indexed by + or − when one polarity is considered.

S_1	first surface used for the Ampère–Maxwell law integration
S_2	second surface used for the Ampère–Maxwell law integration
S_{21}	part of the S_2 surface
S_{22}	part of the S_2 surface
S_{23}	part of the S_2 surface
t_i	inception time of the first corona
U_c	reference voltage used in the first charge–voltage relationship[4]
U'_c	reference voltage used in the second charge–voltage relationship[4]
U_i	inception voltage of the first corona
$U_{i,o}$	minimum inception voltage of the first corona
U_g	axial geometric potential
U_L	potential at the streamer extremity
V	spherical volume where first corona develops
α	semi-angle at the apex of the part of sphere
β	coefficient for α
δ	relative air density
ε_0	dielectric constant of the vacuum
Φ_E	electric flux
μ_0	magnetic permeability of the vacuum
ρ	volume charge density
Ω	solid angle

1. Introduction

The streamer corona observed in the large point-to-plane air gaps submitted to an impulse voltage is the first repeatable phase of the electrical discharge. The relevant literature on the subject is very rich and the original streamer theory proposed by Raether (1964), Loeb and Meek (1941) has been supported by many experimental results. The first corona is an impulse phenomenon characterized by a current pulse with a time to crest in the range of the nanosecond and a total duration of about 300–400 ns. A typical photograph of the first positive corona recorded at the high voltage laboratory of the University of Pau (France) is shown in figure 1.

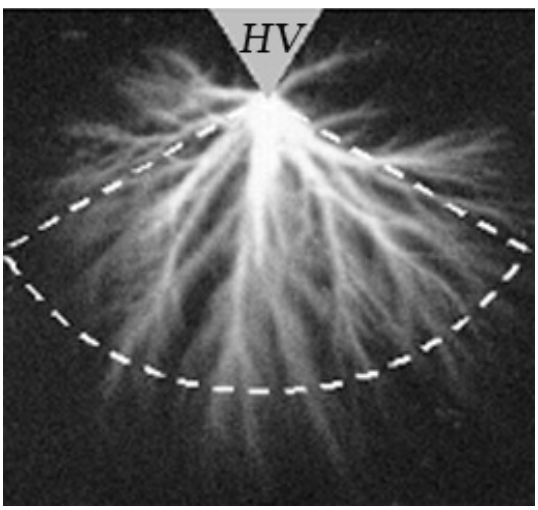

Figure 1. Still photograph of the positive first corona (LGE—University of Pau, France). $R = 0.2$ cm; $D = 50$ cm; $U_i = 140$ kV; $L \approx 20$ cm; $\alpha = 60^\circ$.

The triggering of the first corona pulse, described by the inception voltage U_i, and/or the inception time t_i, is known to be a random phenomenon depending on two conditions: the ambient field in the vicinity of the HV tip electrode and the presence of a free electron suitably localized in this region.

The first condition depends on the pointed electrode shape and requires a minimum voltage $U_{i,o}$ or a minimum inception field $E_{i,o}$. An empirical formula of the corresponding minimum electric field at the tip electrode proposed by Peek (1929) for cylindrical conductors has been adapted by Les Renardières Group (1972) to the rod-plane configuration. Furthermore, this empirical formula is accepted for the two polarities, although the mechanisms are not exactly similar.

The second condition, which is the random component, leads to a random delay of the corona inception time. When an impulse voltage is applied to the air gap, this delay introduces a random 'over-voltage' ($U_i - U_{i,o}$). The greater the rate of rise of the impulse voltage, the lower the delay. The inception probability density has a Poisson-like distribution (Les Renardières Group 1972). If the corona develops after the crest voltage, the inception time t_i is more suitable than U_i to describe the statistical distribution. Based on these two conditions, the 'critical volume model' has been proposed by Les Renardières Group (1972) and then, improved upon by several authors: Allen *et al* (1981), for positive corona and Poli (1982) and Díaz *et al* (1999) for negative corona. This model allows the statistical distribution of U_i or t_i to be estimated.

When the corona develops in the air gap, the streamers propagate in a region where the total electric field (geometric plus space charge fields) is very high. The propagation goes on as long as this total electric field is greater than a minimum value E_{gs}. Under positive polarity the value $5\,\mathrm{kV\,cm^{-1}}$ is commonly admitted. The mean electric field E_s along the streamer channel, after the corona has stopped its development, is also a typical parameter. Phelps (1971) suggested that E_s is of the same order of the guiding field E_{gs} at positive polarity.

The features of the negative corona are more questionable. The first dilemma starts when Raether (1964) and Loeb and Meek (1941) give two different descriptions of the negative streamer channel formation. If the mechanism of propagation is common to the two theories, the channel formation is due to 'retrograde' streamers for Loeb, while, Raether proposes the superposition of the successive avalanches. Suzuki (1975) has experimentally put in evidence what he calls the 'slow' and the 'fast' negative streamers, which confirms that the two mechanisms exist. Reversed streamers during the first negative corona phase have also been observed (Reess *et al* 1995). Gallimberti *et al* (2002) adopted a guiding field $E_{gs} = 7.5\,\mathrm{kV\,cm^{-1}}$. Waters *et al* (1979) proposed a mean field of $10\,\mathrm{kV\,cm^{-1}}$ with a maximum value of $18\,\mathrm{kV\,cm^{-1}}$ near the streamers extremities. Gorin and Shkilev (1976) estimated E_s between 13 and $16\,\mathrm{kV\,cm^{-1}}$.

Various parameters like the length, the diameter and the speed of the corona streamers are available for measurement. For instance, Waters (1987) and Gallimberti (1979) have reported that the variation of the streamer length L is almost linear with the inception voltage U_i as long as L is small compared with the gap length. The ratio was $0.145\,\mathrm{cm\,kV^{-1}}$ for the first author, and $0.152\,\mathrm{cm\,kV^{-1}}$ for the second. A main

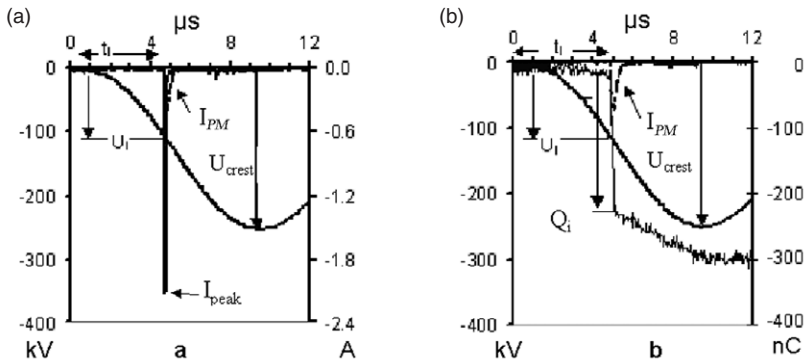

Figure 2. Example of electric signals recorded when the first negative corona develops: (*a*) from current measurement in the HV electrode: $U_i = 110$ kV; $I_{crest} = 2.23$ A; I_{PM} (a.u.), (*b*) from charge measurement in the HV electrode: $U_i = 114$ kV; $Q_i = 214$ nC; I_{PM} (a.u.).

parameter of the first corona is the variation of the charge Q_i on the electrode surfaces due to the ionization phenomena produced in the air gap. The charge Q_i can be an induced and/or a conductive charge but its measurement informs correctly about the actual charge Q_c created and deposited in the gap by the streamers.

The space charge produced by the first corona has already been modelled either with electrostatic models by Wang and Wang (1988), Davies *et al* (1989), Goelian *et al* (1997) or as a consequence of the streamer propagation defined by Raether and Loeb (Dawson and Winn 1965, Phelps 1971, Gallimberti 1972, 1979, Phelps and Griffiths 1976).

Wang and Wang (1988) have proposed a volume charge density of the type $\rho = a/(r + c)^b$ where r is the radial coordinate, the origin being at the tip of the rod electrode and a, b and c three constants chosen to get a constant radial electric field value in the part of sphere occupied by the corona. From the expression of $\rho(r)$, the actual space charge, the induced and the measured charges are calculated. The part of sphere is defined by the semi-angle α at the apex of the part of sphere and the axial length of the axial streamer is deduced from the energy-balance condition defined by Gallimberti (1972). Goelian *et al* (1997) represented the streamer by a charged line with a constant electric field E_s. Thus, the first corona is composed of N streamers with the same line charge density. Davies *et al* (1989) consider an equivalent space charge distributed on a shell ($r = L$) in such a way so as to maintain it as an equipotential surface. They express that the electric field variation on the shell before, $E_g(r = L)$, and just after, E_{gs}, the corona development is proportional to the measured charge and they impose a minimum inception field on the HV surface electrode.

All these parameters are strongly dependent on 'geometric' parameters like the shape and the polarity of the impulse voltage and on the highly non-uniform field distribution, i.e. the gap geometry (tip radius of the pointed electrode R and gap length D). In most cases, the rise of the applied voltage during the 300–400 ns of the streamers propagation is negligible, and only one voltage level is associated with the first corona which is the inception voltage U_i. With regard to polarity, the positive and negative first coronas must be treated separately despite the similarity between the mechanisms of the streamer propagation of both polarities. The positive corona, which develops from a pointed anode, has been better described experimentally than the negative corona which develops from a pointed cathode. Also, the atmospheric conditions like the relative air density δ, the absolute humidity h and the negative or positive ion densities clearly influence the triggering and the development of the first corona.

This work deals with the study of the Q_i–U_i relationship of the first impulse corona. The electrode configuration is a 1 m point-to-plane airgap with various tip radii at the point extremity. The applied voltage is a positive or a negative impulse voltage of equal curve parameters. Artificial variations of some atmospheric parameters have been created to complete the study. The aim of this work is to build a model that can predict the apparent or actual charge created by the first impulse corona at a given inception voltage U_i. First, from the experimental results, two relationships between Q_i and U_i with empirical coefficients can be proposed. Then, the application of two of Maxwell's equations, in a correct approximation, leads to similar relationships giving a physical meaning to the empirical coefficients. These last 'semi-empirical' relationships allow the effect of some atmospheric parameters to be considered.

2. Experimental arrangement

The tests have been performed in the high voltage laboratory of the Technical University of Munich. The high voltage room is a closed climatic chamber with the following dimensions: 5.15 m × 6.45 m × 4.0 m amounting to a 133 m^3 volume. The high voltage electrode is a 30° conical tipped brass rod of $R = 0.2$ cm curvature radius, 1 m distant from the ground plate. The voltage is brought in by a HV bushing from a separate HV laboratory containing a 1-stage impulse generator for 500 kV. The tests have been made under both positive and negative polarity. An inductance has been introduced into the circuit resulting in a unipolar oscillating impulse. The peak voltage and the inductance values could be adjusted to keep the rate of rise of the applied voltage constant and to get the set of first corona parameters recordings in the constant voltage slope region. This rate of rise of the applied voltage is in the range 45–50 kV μs^{-1}.

The recording instrument is a four-channel digital storage oscilloscope: voltage signal U from a damped-capacitive divider, current signal I from a fibre optic system and

photomultiplier signal I_{PM}. The fourth channel is used to monitor the trigger-signal from the impulse-generator's firing gap. Figure 2 shows, in two typical recordings, the shapes of the voltage, PM-trace, current and charge impulses.

The current flow I at the HV cone tip electrode (material: brass) is recorded using a coaxial shunt in parallel with a light emitting diode housed in the shielding body of the HV electrode. The bandwidth of the whole system is 100 MHz.

The charge is either computed by numerical integration of the current signal or measured with a capacitive probe whose signal is transmitted by an opto-electronic system. In fact, the different ways of charge measurements have led to similar results. The measured charge Q_i involved in the present study is associated with the first corona phase. The capacitive component owing to the charge of the electrode system is not registered (see figure 2).

The relative air density δ is always recorded and stays in the range of 0.95–0.98. The natural absolute humidity varies from 4 to 11 g m^{-3}. The negative and positive ion densities recorded by means of a Gerdien ion counter during the day are in the range of 500 to 1200 ions cm^{-3} and the average ratio of negative to positive ion density is 0.9. It must be noted that the Gerdien ion counter is able to record the small ion densities only like O^- or O_2^- (mobility in the range of 0.5–2 cm^2 V^{-1} s^{-1}). The aim of ion measurement is to get the same atmospheric composition before each shot and thus to define the time interval between shots. Additionally, the ion density has been varied to learn about its influence on the charge–voltage relationship. Negative and positive ions have been produced artificially with one or two active small electrodes made of several wires and connected to a dc voltage supply (up to ±20 kV).

The tip radii have been changed and four different tips have been used. The conical body of the electrode remains the same and only the tip extremity is changed. The values of the four tip curvature radii R are: 0.05 (needle), 0.2, 0.5 and 1 cm. The shape of the electrode extremity is detailed in figure 3.

Finally, some experiments performed in the HV laboratory of the University of Pau (France) are taken into consideration in this paper. The HV electrode is identical ($R = 0.2$ cm) but the gap length is reduced to 50 cm. These, photographs of the first impulse corona have been recorded by means of an image converter.

3. Empirical charge–voltage relationships

As was expected, the inception voltage U_i follows a probability distribution dependent on the atmospheric conditions in terms of mean value and standard deviation. In an overview of the data, at positive polarity and for $R = 0.2$ cm, the inception voltages recorded vary from a threshold close to 40 kV up to approximately 240 kV. The associated measured first corona charge Q_i ranges from nearly 0–2200 nC. At negative polarity and the same tip radius, the minimum inception voltage $U_{i,o}$ is close to the positive one and the maximum value can reach 180 kV. The measured negative charge Q_i does not exceed 900 nC. All the coronas were produced in the front of the impulse voltage.

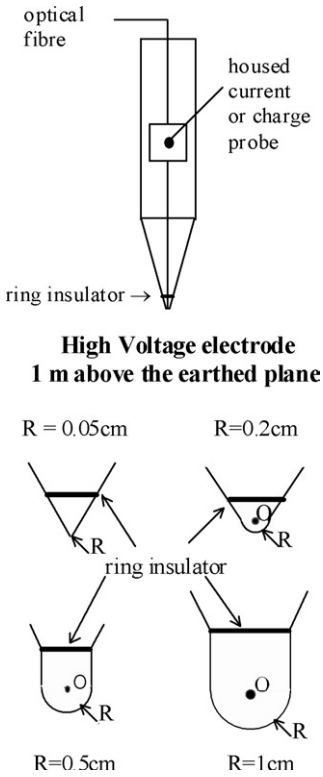

Figure 3. HV electrode and the details of the 4 tips. The O point is the centre of the tip radius.

In order to account for the quadratic form of the charge–voltage relationship, we have plotted $\sqrt{Q_i}$ as a function of U_i. The results obtained for both polarities are shown in figure 4 for the four tip radii. The straight lines are the linear correlations. The coefficient of correlation is very satisfying whatever the tip radius. On the two graphs we can see that the effect of the tip radius is real but quite weak. The slopes of the straight lines increase when the tip radius increases. The effect of the radius is more marked for the smallest radius, especially at negative polarity.

From these experimental data, a quadratic expression appears well adapted to describe analytically the variation of the measured charge Q_i with the inception voltage U_i. Two different quadratic forms have been selected:

$$Q_i = k \cdot U_i \cdot (U_i - U_c) \tag{1}$$

$$Q_i = k' \cdot (U_i - U_c')^n. \tag{2}$$

The pairs of parameters (k, U_c) and (k', U_c') have been deduced by non-linear regression. In spite of their different forms, both relationships describe well the experimental results and correctly fit the experimental data.

In equation (1), the proportion of the variance explained stays close to 1. Nevertheless, it must be noticed that the correlation is more satisfactory at positive polarity.

Equation (2) also leads to a good fit of the experimental results and the coefficient of the proportion of the variance explained stays greater than 0.93 with values of n close to 2 for both polarities. The case $n = 2$ is shown in figure 4.

From an engineering point of view, equation (1) has been preferred first because it presents some practical advantages, at

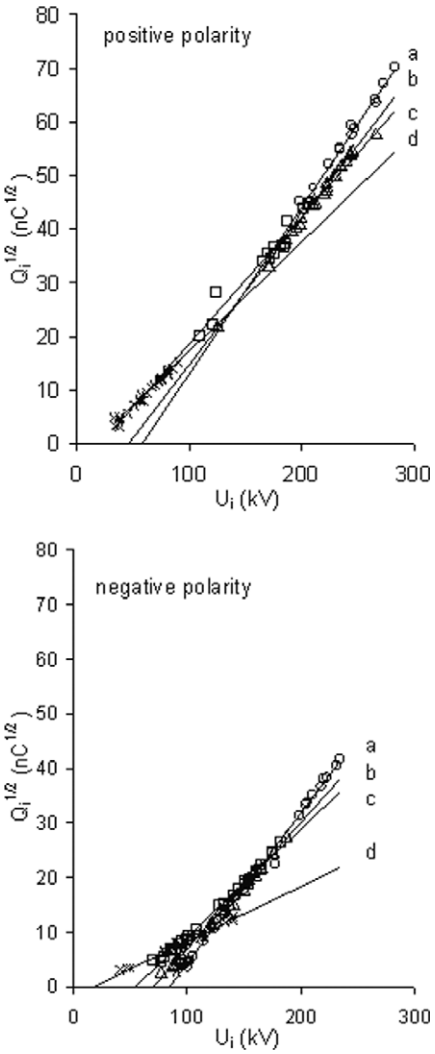

Figure 4. $\sqrt{Q_i}$ versus U_i for the 4 tip radii: (a) $R = 0.05$ cm; (b) $R = 0.2$ cm; (c) $R = 0.5$ cm; (d) $R = 1$ cm; $\delta = 0.96$; $h \approx 4$–5 g m^{-3}.

least at the positive polarity. Indeed, the U_c parameter can be represented by the theoretical minimum inception voltage $U_{i,o}$. This representation holds true for the four tip radii of the pointed electrode we have used. Besides these results with our data, the Q_i–U_i curves given by equation (1) have been tested on experimental data originating from various large airgaps ($D = 1.5$–13.5 m) and similar HV electrodes (Les Renardières Group 1974, Gallimberti 1979) and the fit is still satisfactory for both the equations assuming $U_c = U_{i,o}$. Finally, equation (1) has been used previously by Ortéga *et al* (1994) in order to build a model of leader development in a very large airgap.

Under negative polarity, the assumption $U_c = U_{i,o}$ does not always lead to a proper fit of equation (1) with the experimental data. The U_c values calculated by non-linear regression for the different tip radii exceed the theoretical minimum inception voltages by about 15%.

One should be aware that the measurements from series to series are not strictly repetitive owing to the experimental scatter. The search for the best correlation for both equations (1) and (2) and for each series gives different solutions for the

Table 1. Coefficients deduced from the linear regression of $\sqrt{Q_i}$ as a function of U_i. The + or − index indicates the corona polarity and R is the tip radius.

R (cm)	k'_+ (pC kV^{-2})	U'_{c+} (kV)	k'_- (pC kV^{-2})	U'_{c-} (kV)	k'_+/k'_-
0.05	42	16	10	13	4.2
0.2	61	30	35	44	1.7
0.5	69	40	53	70	1.3
1	88	50	75	84	1.2

(k, U_c) and (k', U'_c) pairs. However, the statistical study shows that k and U_c, on one hand, and k' and U'_c, on the other hand, are strongly dependent on each other and the coefficient of correlation between them is close to 1. As a consequence, the dependence between the two parameters induces a large scatter of each one. This is more pronounced at positive polarity.

Heilbronner *et al* (2003) expressed the linear dependence in equation (1) between k and U_c for $R = 0.2$ cm and for both polarities:

$$k_+ = 0.8 \cdot U_c + 18.2, \tag{3}$$

$$k_- = 0.5 \cdot U_c - 0.7, \tag{4}$$

where k_+ and k_- are expressed in pC kV^{-2} and U_c in kV. The quotient k_+/k_- has an asymptote in 1.6 compared with the value of 1.7 in table 1.

The equation (3) is also valid for the other three tip radii used. Thus, at positive polarity, equations (1) and (3) allow us to predict the charge–voltage relationship in the range of electrode configuration described here. At negative polarity, additional knowledge is needed to determine the physical meaning of U_c, if there is one.

For equation (2), table 1 summarizes the k' and U'_c coefficients obtained from many series by linear correlation when $\sqrt{Q_i}$ as a function of U_i is considered (see figures 4 and 5).

The advantage of equation (2) and the dependence between k' and U'_c will be discussed in section 6.

3.1. Influence of atmospheric parameters

The positive and negative ions were produced artificially in the laboratory by small dc coronas. The Gerdien ion counter, able to record the small ion densities only, indicated ion densities' growths up to 40 000 ions cm^{-3}. The effect of the negative ions upon the charge–voltage relationship is clear. It is well known that a high negative ion density clearly reduces the inception voltage distribution close to the minimum level (Rühling *et al* 1999). In the same way, the charge measured is also reduced in such a way that equations (1) and (2) are not affected and stay valid for both polarities. This can be seen in figure 5 for positive polarity where the effect of the negative ions is more pronounced. Thus, the small negative ions have no sensible effect on the charge–voltage relationship. In return, the influence of the positive ions produced artificially by the dc coronas is not significant, either on the U_i distribution or on the charge–voltage relationship.

Our experiments have been performed during several seasons of the year and we have recorded a natural variation of

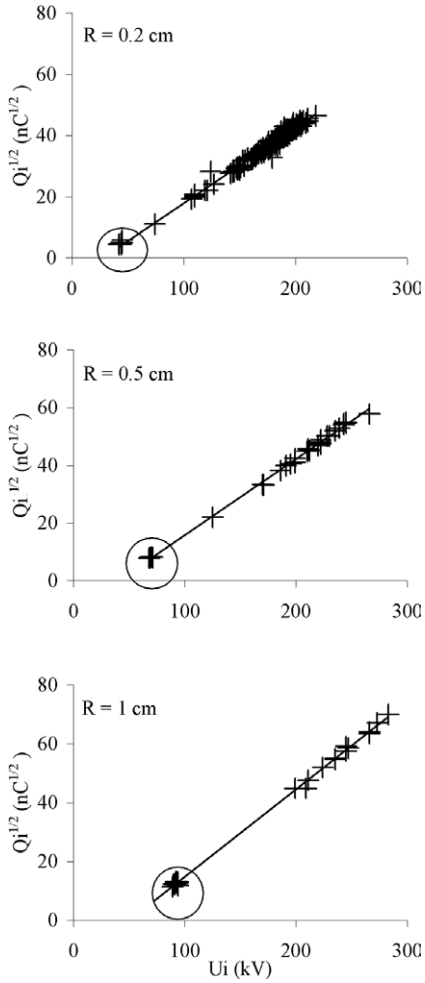

Figure 5. $\sqrt{Q_i}$ versus U_i at positive polarity for 3 different tip radii R; experimental data (+) and equation (2) (−) ($n = 2$); the circles specify the series done with a high negative ion density; $\delta = 0.96$; $h \approx 4$–$5\ \mathrm{g\ m^{-3}}$.

the absolute humidity from 4 to 11 g m^{-3} with a quasi constant relative air density ($0.95 < \delta < 0.98$). It seems that only the scatter of the data, inception voltage U_i and measured charge Q_i is affected by the variation of the humidity.

Our conclusion about the influence of the atmospheric parameters, especially the humidity effect, is that the measurement must be done with great care. For instance, we think that the role of the large ions is important to reach an objective conclusion. A device able to measure the large ion density is under construction and our measurements will be compared with other experiments performed in a tropical country (Argentina). Thus, within the range of the observed absolute humidity, no clear effect upon the charge–voltage relationship has been detected.

4. Gauss's law and charge–voltage relationship

The first corona is assumed to have features resulting in the following four assumptions:

(1) the first corona charge is represented by a continuous charge distribution;

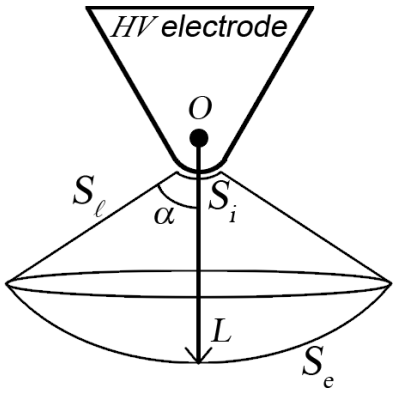

Figure 6. Definition of the part of sphere used for the integration of Gauss's law. S_e: external surface; S_i: internal surface; S_ℓ: lateral surface R' (not marked) and L are the radii of the S_ℓ and S_i surfaces, respectively.

(2) the average electric field E_s inside this distribution is (a) constant whatever the applied voltage U_i, (b) radial with regard to the centre of the tip of the HV electrode and (c) close to the guiding field value E_{gs}—and this holds for both polarities;
(3) the corona extension L is a linear function with U_i as long as the streamers have not reached the earthed plane; and
(4) the first corona roughly develops within a volume V which consists of a part of sphere situated at the centre of the tip of the HV electrode.

The part of sphere is defined by the two radii R' and L and α, the semi-angle at the apex of the part of sphere can be seen in figure 6. The origin of the radial coordinate r is taken at the centre of curvature of the tip of the HV electrode.

The previous assumptions made upon the average electric field E_s impose that the volume charge distribution is in the form: $\rho = A/r$, A being a constant. Indeed, Gauss's law links the electric flux $\Phi(E_s)$ and the volume charge distribution, ρ, as follows:

$$\Phi(E_s) = \int_{S_i} \vec{E}_s \cdot \mathrm{d}\vec{S} + \int_{S_e} \vec{E}_s \cdot \mathrm{d}\vec{S} = \frac{1}{\varepsilon_0} \int_V \rho \cdot \mathrm{d}V,$$

$$\Rightarrow E_s = \frac{A}{2\varepsilon_0} \tag{5}$$

The total actual charge Q_c deposed by the corona in the volume V is:

$$Q_c = \frac{A \cdot \Omega}{2}(L^2 - R'^2), \tag{6}$$

Ω is the solid angle: $\Omega = 2\pi(1 - \cos(\alpha))$.

The capacitive component due to the applied voltage is not taken into account and Q_i results only from the development of the first corona. The Q_i variation is the sum of the collected charge at the electrode plus an induced charge Q_e due to the actual charge deposited in the airgap Q_c. Q_i can be calculated by subtracting Q_e from Q_c (equation (6)). Computing the potential created by Q_c at the HV electrode, Q_e can be expressed as follows:

$$Q_e = A \cdot \Omega \cdot R \cdot (L - R'). \tag{7}$$

So, assuming $R \approx R'$, we have:

$$Q_i = Q_c - Q_e = E_s \cdot \varepsilon_0 \cdot \Omega \cdot (L - R')^2. \tag{8}$$

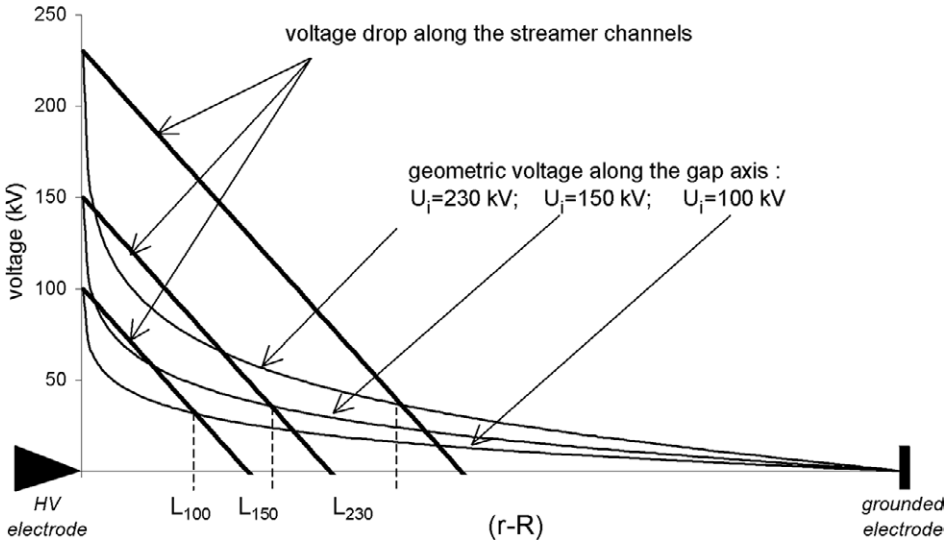

Figure 7. Potential distribution along the gap axis for three inception voltages: ——, geometric voltage (charge simulation method) ——, along the streamers zone. According to Goelian *et al* (1997), the intersections of the curves correspond to the maximal extension of the corona.

Since the electric field in the streamer region has a constant value, the S_e surface can be considered as an equi-potential surface and, in accordance with assumption (2) we can write:

$$(L - R') = \frac{U_i - U_L}{E_s} \tag{9}$$

and thus:

$$Q_i = \frac{\varepsilon_0 \cdot \Omega}{E_s}(U_i - U_L)^2, \tag{10}$$

where U_L is the S_e surface potential and $\Omega = 2\pi(1 - \cos(\alpha))$.

The calculation of U_L depends upon E_s and L. The corona extension L can be calculated with a geometric construction (Goelian *et al* 1997). The axial corona length coincides with the intersection of the axial geometric voltage curve $U_g(r)$ and the $-E_s$ slope line going through U_i (see figure 7). It must be noticed that the streamer length L obtained with this geometric method is indeed proportional to the inception voltage and this reinforces assumption (2). We can note now the similarity between equations (10) and (2). The comparison, the significance of the mean field E_s and the α values will be discussed in section 6.

5. Charge–voltage relationship and the Maxwell–Ampère law

It is interesting to make a new calculation using another of Maxwell's equations which allows us to directly link the measured charge Q_i and the variation of the electric field in the airgap due to the space charge. The integral form of the Maxwell–Ampère law is as follows:

$$\oint_C \vec{B} \cdot \mathrm{d}\vec{\ell} = \mu_0 \cdot I + \mu_0 \cdot \varepsilon_0 \cdot \frac{\partial \Phi_E}{\partial t}. \tag{11}$$

The left term represents the line integral of the magnetic field along the closed curve C. The right term is the total current composed of the steady current passing through any surface S bounded by the closed curve C plus the current of influence given by the time rate of change of the electric flux through the same surface S multiplied by μ_0, and the magnetic permeability of the vacuum (also accepted for air). All the variables are time dependent ($B(t)$, $I(t)$, $\Phi_E(t)$) and the equation (11) is verified at any time.

Let us consider the figure 8. The equation (11) is treated by considering the C contour inside the HV electrode and two different surfaces S_1 and S_2 bounded by C. The C loop encircles the wire collecting the current I during the first corona development. S_1 is the smallest surface bounded by the C contour and $S_2 = S_{21} + S_{22} + S_{23}$ is the association of a part of sphere centred at the O point with a radius equal to L, $S_{21} + S_{22}$, and a tube inside the HV electrode, S_{23}. We can note that S_{22} is similar to the S_e surface of figure 6.

Since the electric field inside the electrode is zero, and thus constant, when considering the S_1 surface, at any time the equation (11) is restricted to:

$$\oint_C \vec{B} \cdot \mathrm{d}\vec{\ell} = \mu_0 \cdot I. \tag{12}$$

When considering the S_2 surface, the electric flux is not zero only through the S_{22} surface. Indeed, the electric field is zero inside the HV electrode and we can assume that S_{21} leans on the external streamers. Furthermore, no charge crosses the S_2 surface and then the equation (11) becomes:

$$\oint_C \vec{B} \cdot \mathrm{d}\vec{\ell} = \mu_0 \cdot \varepsilon_0 \frac{\partial E_L}{\partial t} \cdot S_{22}, \tag{13}$$

where E_L is the total electric field on the S_{22} surface ($r = L$) at any time.

The two left terms in equations (12) and (13) are equal since they represent the same line integral. Then, the two right terms are also equal and, with $S_{22} = S_e$ we obtain:

$$I = \varepsilon_0 \cdot \frac{\partial E_L}{\partial t} \cdot S_e, \tag{14}$$

Using the Maxwell–Ampère law no restrictions are needed for the time dependence. Then we can integrate equation (14)

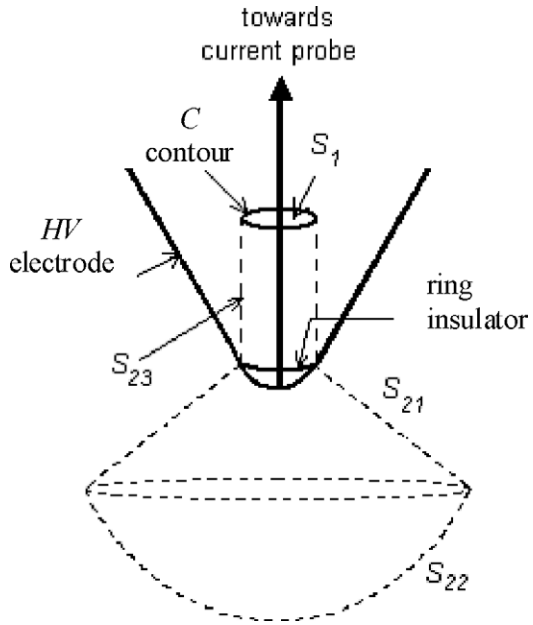

Figure 8. Definition of the C contour and the surfaces used for the integration of the Maxwell–Ampère, law. The line integral of the magnetic field is calculated along the closed curve C and the flux of the current density is calculated through S_1 and through $S_2 = S_{21} + S_{22} + S_{23}$.

during the time development of the first corona from $t = t_i$ to $t = t_i + \Delta t$, Δt being small enough to neglect the increasing rate of the applied voltage.

Thus, I is the total current recorded at the HV electrode and the integration of equation (14) leads to

$$\Delta Q = Q_i = \varepsilon_0 \cdot S_e \cdot \Delta E_L. \tag{15}$$

$\Delta E_L = E_L(t_i + \Delta t) - E_L(t_i)$ is the variation of the electric field on the S_e surface between the beginning and the end of the development of the first corona. $E_L(t_i)$ is the geometric electric field (gap free of charge) and is also assumed to be constant and orthogonal at any point of the S_e surface. Let us call this electric field E_{gL}. Since the positive streamers propagate as long as they are supported by an ambient electric field greater than or equal to a certain critical value E_{gs} and S_e coincide with the limit of the streamer propagation, we can write $E_L(t_i + \Delta t) = E_{gs}$ and then:

$$Q_i = \varepsilon_0 \cdot \Omega \cdot L^2 \cdot (E_{gs} - E_{gL}). \tag{16}$$

Equation (16) cannot be linked directly with the empirical relationships equations (1) or (2), but it allows a calculation of the Q_i charge. Indeed, we have seen that L could be deduced from a geometrical construction and thus, by field calculation with the charge simulation method, the E_{gL} value can be deduced, at least, on the gap axis. For instance, figure 9 shows how E_{gL} varies with the streamer length L. The corresponding U_i values are also displayed and equation (16) can be numerically compared with the experimental Q_i–U_i relationship.

6. Discussion

Compared with the Gauss's law, which links the actual charge and the mean electric field, the Ampère's law

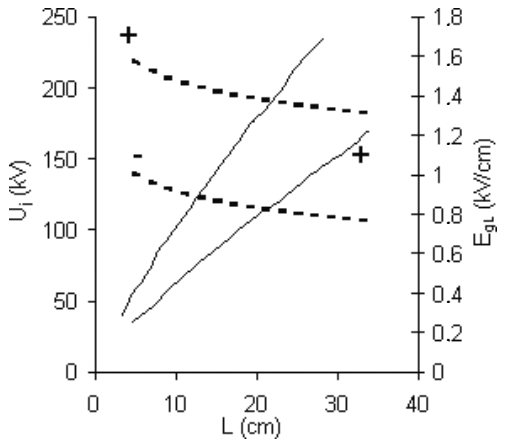

Figure 9. Electrode potential U_i and geometric field $E_{gL}(r = L)$ as a function of the streamer length L for both polarities (+ and −) deduced from the geometric method. $R = 0.2$ cm; $E_{s^+} = 4.5\,\mathrm{kV\,cm^{-1}}$ and $E_{s^-} = 7.5\,\mathrm{kV\,cm^{-1}}$; $\alpha_{max} = 60°$; $\beta = 18$.

correlates the measured charge and the field variation at $r = L$ owing to the first corona development. The equation (10) is closer to equation (2), but equation (16) uses parameters that are more accessible to measurement and need less assumptions. Thus, despite their similarity, it is now interesting to confront the two relationships with the experimental data in order to comment upon the various assumptions.

6.1. Gauss's law

Equation (10) obtained by Gauss's law can be overcome with the empirical equation (2) if we assume that

$$k' = \frac{\varepsilon_0 \cdot \Omega}{E_s} \tag{17}$$

and

$$U'_c = U_L. \tag{18}$$

The relationship 17 can be verified by considering the k' values from table 1 and by adjusting the two parameters which are the semi-angle α and the mean field along the streamers E_s. Phelps (1971) and Dellera and Garbagnati (1990) suggested that E_s is comparable to E_{gs}. The amplitude of this guiding field is $E_{gs^+} \approx 5\,\mathrm{kV\,cm^{-1}}$. At negative polarity, we can extrapolate the equivalence between the two electric fields. For the negative streamers Gallimberti *et al* (2002) proposed $E_{gs^-} \approx 7.5\,\mathrm{kV\,cm^{-1}}$.

In table 1 we have calculated the ratio of the k' values obtained at positive and negative polarities, namely k'_+ and k'_-. For $R = 0.2$ cm this ratio is equal to 1.7. Assuming the same semi-angle α_m for both polarities and $E_{s+} \approx 4.5$ kV (positive corona) this ratio implies a mean negative electric field $E_{s-} \approx 7.5\,\mathrm{kV\,cm^{-1}}$. This value is consistent with the electric field used by Gallimberti *et al* (2002). Thus, the α value can be calculated from the k'_+ and k'_- values of table 1. The angle deduced is $\alpha \approx 60°$. To discuss this value of α we have at our disposal some photographs of the first corona recorded by means of an image converter (figure 1). The pointed electrode has $R = 0.2$ cm tip radius and the gap length is 50 cm. According to the pictures, the α semi-angle often

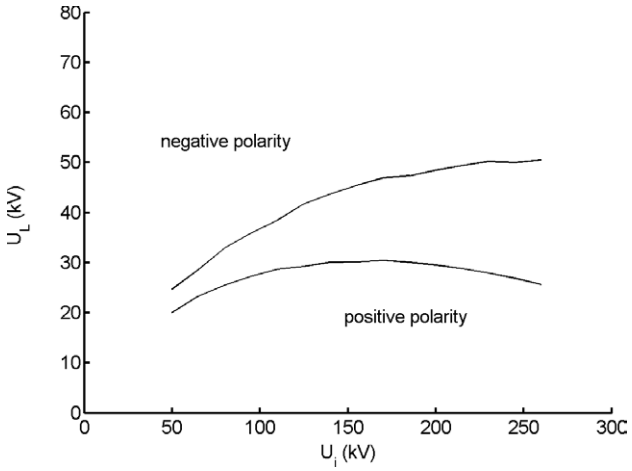

Figure 10. U_L potential at the corona extremity as a function of U_i deduced from the geometric method. $R = 0.2$ cm $E_{s^+} = 4.5\,\mathrm{kV\,cm^{-1}}$ and $E_{s^-} = 7.5\,\mathrm{kV\,cm^{-1}}$; $\delta = 0.96$; $h = 5\,\mathrm{g\,m^{-3}}$.

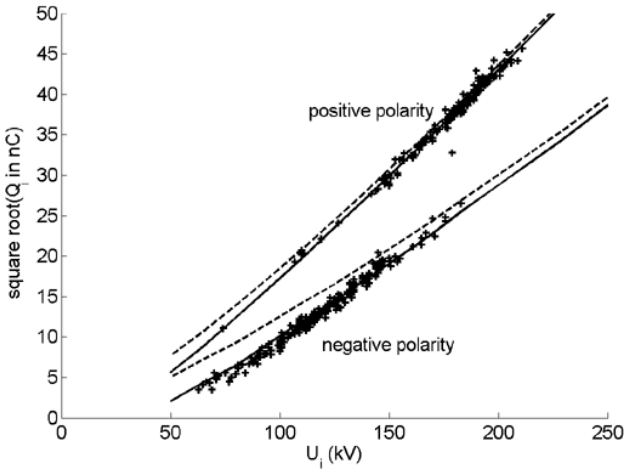

Figure 11. Example of good correlation between equation (10) and experimental data. U_L is deduced from the geometric method plus experimental data: ——, calculated charge with $\alpha = 62^\circ$; · · · · · ·, calculated charge with α from equation (19) with $\alpha_{max} = 62^\circ$ and $\beta = 20$; $R = 0.2$ cm; $E_s = 4.5\,\mathrm{kV\,cm^{-1}}$; $\delta = 0.96$; $h = 5\,\mathrm{g\,m^{-3}}$.

exceeds 90° but in that case the 'horizontal' streamers are much smaller in length than the axial streamers. Thus, the assumption as part of a sphere could be excessive. However, in a first assumption, a mean α_m value can be adopted to consider an equal streamer length whatever its direction of development, and $\alpha_m = 60^\circ$ is coherent with the photographs. Let us notice that Wang and Wang (1988) used a smaller value $\alpha_m = 45^\circ$.

Equations (17) and (18) do not contradict the dependence observed experimentally between k' and U'_c since U_L depends directly upon the E_s value. Furthermore, since Gauss's law states that Q_i is proportional to the external surface of the corona $S_\ell = 2\pi(1 - \cos\alpha)L^2$, L and thus U_L, is linked to Ω.

Equation (18) implies a constant value for U_L in accordance with the experimental results (table 1). Figure 10 shows the calculated values of U_L as a function of U_i for $R = 0.2$ cm. The U_L potential is deduced from the geometric method with $E_{s^+} = 4.5\,\mathrm{kV\,cm^{-1}}$ and $E_{s^-} = 7.5\,\mathrm{kV\,cm^{-1}}$. We note that U_L is clearly U_i dependent. Nevertheless, at positive polarity, the U_L variation is weak enough to get a satisfactory fit between equation (10) and experimental Q_i–U_i curves. In return, at negative polarity, U_L is more dependent upon U_i, and this dependence leads to a bad fit of equation (10) with the experimental results (figure 11). In order to improve this correlation, the variation of the U_L potential can be compensated by a variation of the semi-angle α. We assume that α is U_i or L dependent but cannot express a numerical relationship between these two parameters owing to a lack of photographs of the negative corona. For a first approximation, we propose:

$$\alpha = \frac{\alpha_{max}}{1 + (\beta \cdot R/L)^2}, \tag{19}$$

β being an adjustable coefficient for calculation. The α variation is shown in figure 12 for $R = 0.2$ cm, $\alpha_{max} = 60^\circ$ and $\beta = 18$. The correlation between equation (10) and the experimental data is very satisfying for a range of β values from 15 to 30. Figure 11 shows improvement of the correlation due to equation (19), especially at negative polarity.

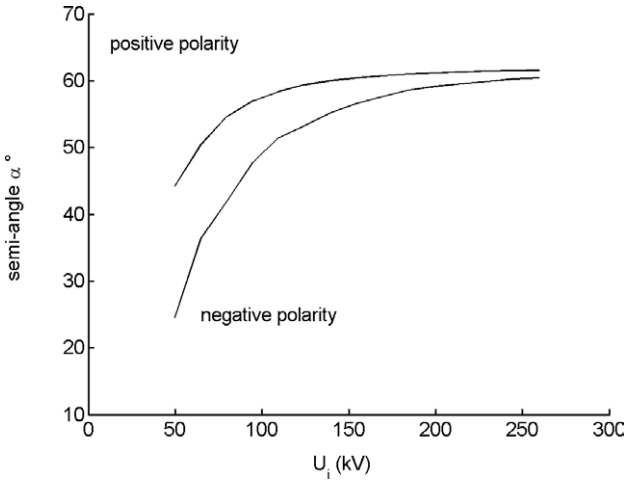

Figure 12. Semi-angle α versus U_i for both polarities: $R = 0.2$ cm; $\alpha_{max} = 60^\circ$; $\beta = 18$.

For the other tip radii, at positive polarity, the fit of equation (10) with the experimental data is also very satisfying conserving the same parameters: $\alpha_{max} = 60^\circ$ and $\beta = 18$ in equation (19) and $E_{s^+} = 4.5\,\mathrm{kV\,cm^{-1}}$. At negative polarity, according to the ratio k'_+/k'_- given in table 1, and assuming $E_{s^+} = 4.5\,\mathrm{kV\,cm^{-1}}$ E_{s^-} decreases to $5.9\,\mathrm{kV\,cm^{-1}}$ and $5.4\,\mathrm{kV\,cm^{-1}}$, respectively, for, $R = 0.5$ cm and 1 cm and increases to $20\,\mathrm{kV\,cm^{-1}}$ for $R = 0.05$ cm. Despite these unexpected values and keeping the equation (19) for the angle ($\alpha_{max} = 60^\circ$ and $\beta = 18$), the fit of equation (10) with the experimental data is also very satisfactory. Another way to reach a good fit is to keep a constant mean field $E_{s^-} = 7.5\,\mathrm{kV\,cm^{-1}}$ and modify α_{max} to 40° for $R = 0.05$ cm, to 80° for $R = 0.5$ cm and to 90° for $R = 1$ cm.

6.2. Ampère's law

In equation (16) three electric fields are involved: the guiding electric field E_{gs}, the mean electric field along the streamers E_s

(through the L calculation) and the geometric field at the corona extremity E_{gL} (at $r = L$). The mean field E_s is still considered equal to the streamer propagation field E_{gs} (Phelps 1971, Dellera and Garbagnati 1990). Then, L being deduced from the geometric method and the charge simulation method allowing the geometric field to be computed anywhere in the gap, E_{gL} can be calculated.

Therefore, equation (16) allows a Q_i–U_i curve to be drawn. Nevertheless, considering the same parameters (E_s, α_{max}, β) this Q_i–U_i curve is not identical to the curve obtained with equation (10). To find the reasons for the disagreement we have to compare analytically the two equations. Thus, the following relationship is deduced:

$$\left(\frac{L}{L-R}\right)^2 = \frac{E_s}{E_{gs} - E_{gL}}. \tag{20}$$

Effectively, assuming $E_s = E_{gs}$ and computing L and E_{gL} as described previously, equation (20) is not correct. But, this relationship can be verified either by considering a slight difference between E_s and E_{gs} or by distinguishing R and R' (the radius of the inner surface considered for the integration of Gauss's law, equation (9). The former leads to a ratio $E_s/E_{gs} \approx 0.85$ and introduces a slight difference between the two fields. The latter leads to the following relationship:

$$R' = R + a \cdot L. \tag{21}$$

The two terms of equation (20) are equal in a 95% interval confidence if R is replaced by R' and $a = 0.125 \pm 0.025$. Equation (21) is justifiable by considering the formation of a more conductive region near the tip. This region may correspond to the stem of the corona which is considered as the leader initiation.

Thus, using equations (19) and (21) and assuming $E_s = E_{gs}$, equation (16) is identical to equation (10) and, at positive polarity, the fit is very satisfactory for the 4 tip radii. In return, at negative polarity, for equation (10), an agreement with the experimental data needs to consider E_s, and thus E_{gs}, different from the admitted experimental values.

We observe that, to simplify the calculation, another assumption can be made. Figure 13 shows that, despite the non-uniformity of the electric field in the air gap, the equi-field lines coincide with the spherical lines centred at the tip centre. The calculation along the gap axis is enough to solve equation (16).

6.3. Humidity influence

Even though our experiments have not yet led to a clear conclusion about the effect of humidity, we may discuss this parameter with the help of equations (10) and (16). It is acknowledged that the space charge created by the positive first corona is reduced when humidity increases, but the quantitative relationship between Q_c or Q_i and h is still ambiguous for large air gaps. Davies *et al* (1989), using a 20 cm gap placed in a shielded chamber with controlled humidity, have found a clear reduction of the total charge of the primary corona with increase in humidity. It should be noted, however, that the primary corona includes several single coronas and not the first one only.

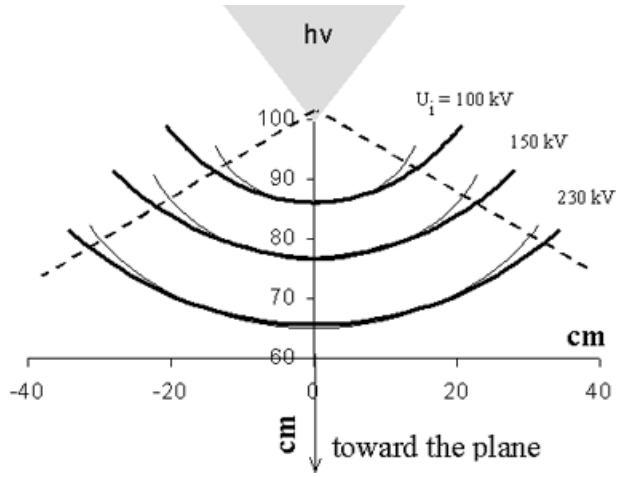

Figure 13. Three equi-fields lines (5 kV cm^{-1}) computed by the charge simulation method for 3 inception voltage levels and compared with 3 parts of circles centred at the tip centre O.

Allen and Dring (1984) have also observed a reduction in the transfer charge at the plane after corona development owing to a humidity increase despite a large scatter in the results. By testing a 1.5 m hemisphere-plane gap, Les Renardières Group (1977) have found a rate of change of −13.5% per g m^{-3}. Hahn *et al* (1976) proposed a rate of −0.9% per g m^{-3} by applying switching impulses on a 50 cm rod-plane gap. Topalis *et al* (1988), in a very similar test configuration, have reported a rate of −0.3 nC per g m^{-3} but, at the same time, a slight decrease in the inception voltage with a rate of −0.9% per g m^{-3}.

The experimental results published by Phelps and Griffiths (1976) indicate that the stability field E_{gs} depends upon absolute humidity and gas pressure. Various experimental studies are available to express the positive guiding field including relative air density and humidity correction factors. Davies *et al* (1989), in their model, have used an expression with the two parameters (E_{gs} in kV cm^{-1}, h in g m^{-3}):

$$E_{gs} = 4.25 \cdot \delta^{1.5} + \frac{(4 + 5\delta) \cdot h}{100}. \tag{22}$$

For example, $h = 5$ g m^{-3} and $\delta = 0.96$ gives $E_{gs} = 4.44$ kV cm^{-1}.

Through this expression k', U_L, E_s and E_{gL} are linked to the absolute humidity. An increase of h leads to a decrease of k'. For instance, a h-variation from 4 to 11 g m^{-3} leads to a decrease of 18% in the calculated charge for a given U_i level. This ratio is compatible with the rate found by Topalis *et al* (1988) but cannot explain the larger decrease in the charge published by Les Renardières Group (1977).

7. Conclusion

From experiments we have shown that a quadratic relationship is convenient to describe the dependence between the applied voltage U_i and the measured charge Q_i of the first corona. This relationship truly exists and has been observed whatever the polarity of the applied voltage, for different tip radii and

with various atmospheric conditions. It has become evident also that the Q_i–U_i relationship depends on one parameter only. Nevertheless, the use of two parameters has allowed the deduction of empirical expressions where these parameters are linked to the electrode configuration. Thus, a generalization of the relationship can be envisaged.

Furthermore, an attempt at a physical interpretation has shown that the quadratic relationship can be justified by assuming a spherical symmetry for the electrode configuration, at least in the vicinity of the gap axis. Indeed, with such an assumption, Gauss's law is easily applicable and a relationship between the electric flux and the charge corona can be established. Then, the Q_i–U_i quadratic relationship is obtained by considering previously observed characteristics of the first corona such as a radial and constant electric field in the corona region and a linear relationship between the inception voltage and the corona extension. On the other hand, the Ampère–Maxwell law has been used to link the measured charge to the variation of the electric flux through a virtual surface, which coincides with the external surface of the first corona. Contrary to Gauss's law, the Ampère–Maxwell law only requires knowledge of the electric field on the external surface, an advantage which reduces the incertitude of the assumptions.

As a conclusion, we can set forth the idea that our calculations will hold and thus be exploitable, as long as the electrode geometry allows a spherical symmetry to be considered, at least in the region where the first corona develops. We think that, at positive polarity, the domain of validity is large in terms of electrode geometry and impulse voltage shape. With respect to negative polarity, we think that the domain of validity will be limited owing to the more complex mechanism of the negative streamer propagation.

Finally, the influence of the atmospheric parameters has not been definitively included in our calculations. If the ion density can modify the inception voltage or charge distribution, the Q_i–U_i relationship is not significantly affected. The charge and inception voltage recordings sometimes differ unexplained under identical atmospheric conditions, suggesting the effect of covert parameters, e.g. large ions. It is essential to work towards discovering them.

Acknowledgments

The authors thankfully acknowledge the financial support of the Deutsche Forschungsgemeinschaft (DFG), Bonn and the Consejo Nacional de Investigaciones Cientificas y Tecnicas (CONICET), Buenos Aires. They also appreciate the guidance of Dr Iain McAllister, Institut for Elteknik, Danmarks Tekniske Universitet, Lyngby.

References

Allen N L, Berger G, Dring D and Hahn D 1981 Effects of humidity on corona inception in a diverging electric field *IEE Proc.* **128** 565–70

Allen N L and Dring D 1984 Effect of humidity on the properties of corona in a rod-plane gap under positive impulse voltages *Proc. R. Soc. Lond.* A **396** 285–95

Davies A J, Dutton J, Turri R and Waters R T 1989 Predictive modelling of impulse corona in air at various pressures and humidities *6th Int. Symp. on Highvoltage Engineering (New Orleans)* pp 189–92

Dawson G A and Winn W P 1965 A model for streamer propagation *Z. Phys.* **183** 159–71

Dellera L and Garbagnati E 1990 Lightning stroke simulation by means of the leader progression model. Part I: Description of the model and evaluation of exposure of free-standing structures *IEEE Trans. Power Delivery* **5** 2009–22

Díaz R R, Rühling F, Heilbronner F and Ortéga P 1999 The corona inception under negative impulse voltage in inhomogeneous fields *11th Int. Symp. on Highvoltage Engineering (London)* vol 3, pp 155–8

Gallimberti I 1972 A computer model for streamer propagation *J. Phys. D: Appl. Phys.* **5** 2179–89

Gallimberti I 1979 The mechanism of the long spark formation *J. Physique Coll.* **7** (Suppl.) C7

Gallimberti I, Bacchiega G, Bondiou-Clergerie A and Lalande P 2002 Fundamental process in long airgap discharges *C. R. Physique* **3** 1335–59

Goelian N, Lalande P, Bondiou-Clergerie A, Bacchiega G L, Gazzani A and Gallimberti I 1997 A simplified model for the simulation of positive-spark development in long air gaps *J. Phys. D: Appl. Phys.* **30** 2441–52

Gorin B N and Shkilev A V 1976 Electric discharge development in long bar-plane in the presence of negative impulse voltage *Elektrichestvo* **6** 31–9

Hahn G, Zacke P, Fisher A and Boecker H 1976 Humidity influence on switching impulse breakdown of a 50 cm rod-plane gap *IEEE Trans. Power Appar. Syst.* **95** 1145–52

Heilbronner F, Rühling F and Ortéga P 2003 Discharge inception under impulse voltage: influence of the lab air ion density and resulting charge–voltage relationship *Proc. 13th Int. Symp. on Highvoltage Engineering (Delft)* p 493

Les Renardières Group 1972 Analysis of the first impulse corona *Electra* **23** 53–68

Les Renardières Group 1974 Research on long air gaps discharges at Les Renardières: 1973 results *Electra* **35** 124–8

Les Renardières Group 1977 Positive discharge in long airgaps at Les Renardières: 1975 results and conclusions *Electra* **53** 31–128

Loeb L B and Meek J M 1941 *The Mechanism of the Electric Spark* (Stanford: Stanford University Press)

Ortéga P, Domens P and Gibert A 1994 Predictive modelling of leader propagation under standard and oscillatory waveshapes *J. Phys. D: Appl. Phys.* **27** 1–9

Peek F W 1929 *Dielectric Phenomena in Highvoltage Engineering* (New York: McGraw-Hill) pp 52–80

Phelps C T 1971 Field-enhanced propagation of corona-streamer *J. Phys. Res.* **76** 5799–806

Phelps C T and Griffiths R F 1976 Dependence of positive corona streamer propagation on air pressure and water vapour content *J. Appl. Phys.* **47** 2929–34

Poli E 1982 A comparison between positive and negative impulse corona *7th Int. Conf. on Gas Discharges (London)* pp 132–5

Raether H 1964 *Electron Avalanches and Breakdown in Gases* (London: Butterworths)

Reess T, Ortéga P, Gibert A, Domens P and Pignolet P 1995 An experimental study of negative discharge in a 1.3 m point-plane air gap: the function of the space stem in the propagation mechanism *J. Phys. D: Appl. Phys.* **28** 2306–13

Rühling F, Heilbronner F, Díaz R and Ortéga P 1999 Laboratory-relevant corona inception of a 1 m-airgap under impulse voltage *11th Int. Symp. on Highvoltage Engineering (London)* vol 3, pp 39–42

Suzuki T 1975 Breakdown process in rod-to-plane gaps with negative switching impulses *IEEE Trans. Power Appar. Syst.* **94** 1381–9

Topalis F V, Katsabekis Th, Bourkas P D and Stathopulos I A 1988 Corona inception and breakdown in medium air gaps under

switching impulse voltages *9th Int. Conf. on Gas Discharges (Venezia)* pp 467–70
Wang W and Wang H 1988 A new model for simulating the effects of space charge in gas discharge *2nd Int. Conf. on Properties of Dielectric Materials (Beijing)* pp 209–11
Waters R T 1987 *Electrical Breakdown in Gases* ed J M Meek and J D Craggs (New York: Wiley) pp 433–522
Waters R T, Allibone T E, Dring D and Allen N L 1979 The structure of impulse corona in a rod/plane gap: the negative corona *Proc. R. Soc. Lond.* A **367** 321–42